Synthetic boundary conditions for compressible near wall turbulence with POD reconstruction

Ye HONG[1,2], Bérengère PODVIN[2], Christian TENAUD[2], Edouard AUDIT [1]

1. Maison de la Simulation, CEA, CNRS, Université Paris-Saclay, Bâtiment 565 Digiteo CEA Saclay, 91191 Gif-sur-Yvette cedex, France
2. LIMSI, CNRS, Université Paris-Saclay, bât 507 Rue du Belvedère, 91405 Orsay cedex

Abstract

Direct Numerical Simulation of turbulent boundary layers requires a high spatial resolution specially near the wall to capture the different length scales inherent of turbulence. To reduce the computing cost related to the high spatial resolution, we investigate techniques that bypass the wall region by using an artificial boundary condition at the bound of a reduced computational domain. A reconstruction strategy based on POD is implemented in order to generate synthetic boundary conditions such that the correct spatial characteristics and dynamics of the turbulence are recovered in the core region of the channel. The boundary condition was tested at two different heights. Statistics in the reduced channel were compared with those of a reference case. A good agreement is observed for the mean velocity profile and shear stresses. The procedure was found to be robust with the boundary height.

Key words : Turbulence, Compressible flow, POD reconstruction, Synthetic boundary condition, Channel flow.

1.Introduction

Direct Numerical Simulation (DNS) of turbulent boundary layers requires a high spatial resolution specially near the wall to capture the different length scales inherent of turbulence. It was shown that the number of grid points N should vary as $N \sim Re^{\frac{13}{7}}$ in the case of a well-resolved Large-Eddy Simulation (LES) and $N \sim Re^{\frac{37}{14}}$ in the case of a DNS [1]. This makes it difficult to carry out resolved simulations at very high Reynolds numbers. To adress this issue, a number of solutions have been implemented. Classical solutions are generally based on the introduction of a wall model. Park and Moin [2] used a dynamic eddy viscosity model that corrects the effect of the resolved Reynolds stress on the skin friction. Piomelli and Balaras[3] developed an attractive alternative to compute high-Reynolds number flows by using a wall-layer model in LES in which only the outer layer is resolved.

The idea pursued here is different since it focuses on the construction of modeled boundary conditions applied into the inner wall region. In this approach the flow is computed in a reduced numerical domain, which excludes the costly wall region, and where a nonstationary boundary condition on the velocity field at the horizontal edge of the domain is defined at each time step. This procedure has been implemented in the incompressible framework, where the velocity field needs to be imposed on the entire domain

boundary. Podvin and Fraigneau [6] proposed a Proper-Orthogonal-Decomposition(POD)-based wall boundary condition to generate the synthetic field on the boundary. A good agreement of the statistics with turbulent flows in full channels was obtained for several Reynolds numbers. Mizuno and Jiménez [10] proposed a much simpler method, where the boundary condition was obtained from direct rescaling of a velocity field on a plane at the interior of the reduced channel. Although they were able to recover the logarithmic behavior of the velocity profile, a displacement of the profile was observed : their simpler condition was not able to lead to correct turbulent statistics.

The goal of the present work is to extend the POD-based approach developed for incompressible flows to the compressible framework. This could be seen as a first step towards the simulation of coupled physical phenomena. A key aspect of the compressible formulation is that, unlike the incompressible (elliptic) case, waves can propagate through the boundaries, in particular for the density and the pressure, so that the boundary conditions have to be adapted, using the method of characteristics. Some variables on the boundary can be directly recovered from the inside of the domain, while others will need to be prescribed. The idea is to use POD to construct the desired field on the boundary. POD consists in representing the field as the superposition of spatial modes whos amplitude is time-dependent. The shape of the modes is assumed to be known *a priori*. The challenge is then to determine the correct amplitude of the modes.

In the present paper the procedure is applied to a compressible channel at $R_\tau = 180$.

The paper is organized as follows : the numerical method and the boundary conditions are described in the next section. The reconstruction procedure of the synthetic field on the boundary of the reduced channel is described in section 3. Analyses of the results obtained in the reduced channel for $Re_\tau = 180$ are presented in section 4. Conclusion and prospect are finally discussed.

2. Reference Flow Configuration

We consider the direct numerical simulation of a compressible turbulent plane channel flow.

2.1 Equations and numerical scheme

The flow obeys the compressible Navier-Stokes equations :

$$\begin{aligned}
&\frac{\partial \rho}{\partial t} + \frac{\partial}{\partial x_j}(\rho u_j) = 0 \\
&\frac{\partial}{\partial t}(\rho u_i) + \frac{\partial}{\partial x_j}(\rho u_i u_j) + \frac{\partial p}{\partial x_i} = \frac{\partial \tau_{ij}}{\partial x_j} \\
&\frac{\partial \rho E}{\partial t} + \frac{\partial}{\partial x_j}((\rho E + p)u_j) = \frac{\partial}{\partial x_j}\tau_{ij}u_i - \frac{\partial}{\partial x_j}q_j,
\end{aligned} \tag{1}$$

where E is the total energy, T the static temperature, μ the dynamic viscosity, τ the viscous stress tensor, and q the heat flux that are expressed as :

$$
\begin{aligned}
E &= \frac{p}{\rho(\gamma-1)} + \frac{1}{2}u_j u_j \\
\tau_{ij} &= \frac{\mu(T)}{Re}\left(\frac{\partial u_i}{\partial x_j} + \frac{\partial u_j}{\partial x_i} - \frac{2}{3}\delta_{ij}\frac{\partial u_k}{\partial x_k}\right) \\
T &= \gamma {M_0}^2 \frac{p}{\rho} \\
\mu(T) &= \mu_\infty \left(\frac{T}{T_\infty}\right)^{\frac{3}{2}} \left(\frac{110.4 + T_\infty}{110.4 + T}\right) \\
q_j &= -\frac{\mu(T)}{(\gamma-1)RePr{M_0}^2}\frac{\partial T}{\partial x_j}
\end{aligned}
\tag{2}
$$

The resolution of the Navier-Stokes equations (1) has been performed with the in-house parallel (MPI) DNS solver CHORUS, which is developed at LIMSI. The ability of the CHORUS code to compute high Reynolds compressible flows has been established for various test-cases in previous studies (see for instance [7, 8]). The resolution is based on a finite volume approach. An operator splitting procedure is employed that splits the resolution into the Euler part and the viscous problem. The Euler part is discretized by means of a high-order coupled time and space scheme, named OS7 scheme [7] based on a Lax-Wendroff approach, which ensures a 7th-order accuracy in both time and space. Besides, the space discretization of the diffusive fluxes is obtained by means of a classical 2nd-order centered scheme that has been coupled to a 2nd-order Runge-Kutta time integration giving at last a second order accurate scheme in both time and space.

Figure 1 presents the flow configuration and the computational domain. The streamwise, spanwise, and wall normal directions of the flow will be respectively denoted by x, y, and z ; the corresponding components of the velocity are u, v and w. Periodic boundary conditions are applied in both the streamwise and the spanwise directions. The solid walls at the lower and upper parts of the domain are maintained at a prescribed temperature (T_w). The dimensions of the channel are $(Lx, Ly, Lz) = (2\pi, \frac{4\pi}{3}, 2)$. The Reynolds numbers based on the friction velocity (u_τ) and the channel half-height (H) is $Re_\tau = 180$. The Mach number is set to $Ma = 0.5$.

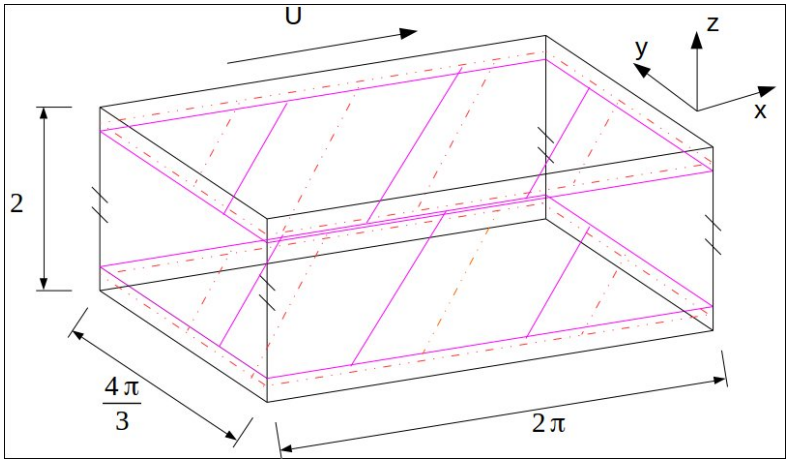

FIGURE 1 – Flow configuration in the channel and computational domain : full domain in black and reduced channel in red.

The flow was integrated from a perturbed laminar profile and allowed to develop in time until statistical convergence was reached, which corresponds to about 700 convective time units H/U_0, where H is the channel height and U_0 is the velocity in the center of the channel.

2.2 Treatment of Boundary conditions

We will denote the variables $[Q_1, Q_2, Q_3, Q_4, Q_5] = [\rho, \rho u, \rho v, \rho w, \rho e]$. As far as compressible flows are considered, the boundary conditions for these fields must fulfill the compatibility relationships based on the Riemann invariants. Considering a boundary normal to the z direction, the Navier-Stokes equations are projected onto the eigenvectors of the Jacobian of the Euler flux in the z -direction. Depending on the sign of the eigenvalues for this Euler flux Jacobian, either the quantity is prescribed when the eigenvalue is positive, or equations of the Riemann invariant are solved by up-winding the Euler flux discretization in the normal to the boundary plane z-direction when the eigenvalue is negative. More precisely, for each point (x, y) of the boundary plane $z = z_0$:

- For the three first eigenvalues w :
  - when $w(x, y, z_0, t^m) > 0.$: $\left\{ \begin{array}{rcl} \rho.u(x, y, z_0, t^{(m+1)}) & = & Q_2^{Est}(x, y, z_0, t^{(m+1)}); \\ \rho.v(x, y, z_0, t^{(m+1)}) & = & Q_3^{Est}(x, y, z_0, t^{(m+1)}); \\ e(x, y, z_0, t^{(m+1)}) & = & Q_5^{Est}(x, y, z_0, t^{(m+1)}); \end{array} \right.$
  - otherwise, the equation of the three first Riemann invariants are solved.

- For the fourth eigenvalue $w + C$ (C is the local speed of sound) :
  - when $w(x, y, z_0, t^m) + C > 0.$: $\rho.w(x, y, z_0, t^{(m+1)}) = Q_4^{Est}(x, y, z_0, t^{(m+1)})$;
  - otherwise, the equation of the fourth Riemann invariant is solved.

- For the fifth eigenvalue $w - C$:
  - when $w(x, y, z_0, t^m) - C > 0.$: $\rho(x, y, z_0, t^{(m+1)}) = Q_1^{Est}(x, y, z_0, t^{(m+1)})$;
  - otherwise, the equation of the fifth Riemann invariant is solved.

In the reference channel, the horizontal boundaries of the domain are walls so the prescribed velocity field is zero. The question is to define an appropriate boundary condition in the reduced channel.

3. Synthetic boundary condition

3.1 Snapshot-POD in Synthetic

In order to prescribe a field Q on the boundary, we rely on Proper Orthogonal Decomposition, that is we express the field as a combination of spatial structures, the amplitude of which varies in time

$$Q(x, y, z, t) = \sum_n \alpha^{(n)}(t)\Phi_Q^{(n)}(x, y, z), \tag{3}$$

Decompositions can be carried out for any selection of components of Q. In what follows, we will use three decompositions : one for ρ (Q_1), one for $\rho\underline{u}$ (Q_2, Q_3, Q_4), and one for $\rho e(Q_5)$.

The spatial structures are obtained from a database of N instantaneous field samples or snapshots following the method of snapshots [11]. The time correlation matrix between each snapshot $\mathbf{Q}(t_i)$ of the

database ($i = 1, \dots N$) are computed following :

$$C(t_i, t_j) = \frac{1}{N} \int_\Omega Q(x, y, z, t_i) \cdot Q(x, y, z, t_j)\, d\Omega. \tag{4}$$

where Ω is the spatial domain where the decomposition is applied. In all that follows Ω will be the half-channel, which corresponds to the fully developed turbulent boundary layer.

The temporal eigenfunctions are recovered by solving a discretized version of the Fredholm equation :

$$C_k(t_i, t_j) \cdot \alpha^{(n)}(t_j)) = \lambda^{(n)} \alpha^{(n)}(t_i). \tag{5}$$

$\lambda^{(n)}$ is the eigenvalue of the nth-mode, corresponding to the energy contained in this POD mode.

and the modes are then recovered using

$$\Phi_q^{(n)}(x, y, z) = \sum_j \alpha^{(n)}(t_i) Q(x, y, z, t_i). \tag{6}$$

Normalized as so, the spatial POD modes form an orthogonal basis. For a given set of modes Φ_q^n, the amplitude of the field at time t is given by

$$\alpha^{(n)}(t) = \int_\Omega Q(x, y, z, t) \cdot \Phi_Q^{(n)}(x, y, z) d\Omega. \tag{7}$$

In all that follows we assume that the modes Φ_q are known *a priori* from the reference simulation. All we need to do to construct the synthetic boundary condition is to determine the amplitude $\alpha⌊n)(t)$.

3.2 Amplitude estimation

From the solution obtained in the reduced channel at the time $t^m = m \cdot \delta t$, we must estimate the POD temporal coefficients to reconstruct the boundary conditions at time $t^{(m+1)} = (m + 1) \cdot \delta t$. This is achieved through projecting the solution at time $t^m = m.\delta t$ onto the POD spatial eigenfunctions on the reduced domain, following the procedure developed in [6]. Let Ω_{red} be the reduced numerical domain. Ω_{red} is the portion of channel extending from a given height within the wall layer up to the half-height of the channel. We have

$$\begin{aligned} b_k^{(n)} &= \int_{\Omega_{red}} Q_k(x, y, z, t^m) \cdot \Phi_k^{(n)}(x, y, z)\, d\Omega_{red}, \\ &\sim \int_{\Omega_{red}} \sum_l \alpha_k^{(l)}(t^m)\, \Phi_k^{(l)}(x, y, z) \cdot \Phi_k^{(n)}(x, y, z)\, d\Omega_{red}, \\ &\sim \sum_l \alpha_k^{(l)}(t^m).R_k^{(l,n)}, \end{aligned} \tag{8}$$

where $R_k^{(l,n)}$ is the dot product between spatial eigenfunctions

$$R_k^{l,n} = \int_{\Omega_{red}} \Phi_k^{(l)}(x, y, z) \cdot \Phi_k^{(n)}(x, y, z)\, d\Omega_{red}. \tag{9}$$

If we let Ω_{red} coincide with Ω, then $R_k^{(l,n)} = \delta_{ln}$.

Keeping only the largest terms, the estimated temporal coefficients ($\alpha^{P}{}_k^{(n)}(t^{(m+1)})$, can be calculated

from the following approximation :

$$\begin{aligned} \alpha^{P}{}_{k}^{(1)}(t^{(m+1)}) &= \frac{b_k^{(1)}}{R_k^{(1,1)}}, \\ \alpha^{P}{}_{k}^{(n)}(t^{(m+1)}) &= \frac{b_k^{(n)} - R_k^{(n,1)}\alpha^{P}{}_{k}^{(1)}}{R_k^{(n,n)}} \end{aligned} \tag{10}$$

which allows reconstruction of the field on the boundary as :

$$Q_k^P(x, y, z_0, t^{(m+1)}) = \sum_n \alpha^{P}{}_{k}^{(n)}(t^{(m+1)})\Phi_k^{(n)}(x, y, z_0). \tag{11}$$

The approximation is valid as long $R_k^{(n,n)}$ is large enough. A threshold was therefore applied : if the diagonal term was lower than the threshold for a mode n, the estimate for $\alpha^{(n)}$ was set to zero. In the following, the threshold value is set to $\varepsilon = 0.3$.

Once values of $Q_k^P(x, y, z_0, t^{(m+1)})$ are calculated on the boundary planes through equation (11), a rescaling procedure is applied so that the rms value of the field on the boundary matches the reference value at all times. We define a rescaling coefficient (f_{kQ}) as

$$f_{kQ} = \frac{Q_{k_{rms}}^{DNS}}{Q_{k_{rms}}^{P}}, \tag{12}$$

where $Q_{k_{rms}}^{DNS}$ is the rms values of the DNS, and $Q_{k_{rms}}^{P}$ is the spatial rms estimated on the boundary plane :

$$Q_{k_{rms}}^{P} = \sqrt{\frac{1}{Nx \times Ny}\sum_{x,y}(Q_k^P(x, y, z_0, t^{(m+1)}) - Q_{k_{mean}}^{P})^2}.$$

The reconstructed field at the new time step is then given by

$$Q_k^{Est}(x, y, z_0, t^{(m+1)}) = (Q_k^P(x, y, z_0, t^{(m+1)}) - Q_{k_{mean}}^{P}) \times f_{kQ} + Q_{k_{mean}}^{P}, \tag{13}$$

where $Q_{k_{mean}}^{P}$ is the horizontally averaged value of the reconstructed POD field on the boundary plane :

$$Q_{k_{mean}}^{P} = \frac{1}{Nx \times Ny}\sum_{x,y} Q_k^P(x, y, z_0, t^{(m+1)}). \tag{14}$$

An organization chart of the simulation procedure in the reduced channel with the synthetic boundary conditions is given in Figure 2.

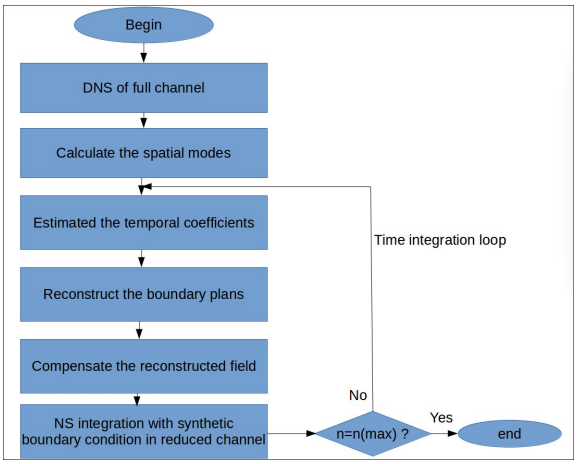

FIGURE 2 – Organization chart for synthetic boundary conditions in the reduced channel.

3.4 Practical Implementation

As mentioned above, we chose to use three snapshot POD decompositions : two scalar POD decompositions, one for the density (ρ), and one for the internal energy ($e = E - \frac{1}{2}\mathbf{u}\cdot\mathbf{u}$), and a vectorial POD decomposition for the momentum vector ($\rho\mathbf{u}$). Other combinations of the variables decomposed were tested and tended to give equal or worse errors.

The POD was performed on 100 sampled snapshots taken over 625 time units (H/U_∞) from the DNS of the full channel flow. The first snapshot was take after statistical convergence has been reached, after about 700 time units. To increase the number of events in the sampled snapshots, fields the lower and upper parts of the channel has been assumed. Due to storage requirements, we selected all the POD modes (*i.e.* 200 modes) for the scalar decompositions while only 128 POD modes were selected for the momentum corresponding to more than 80 % of the kinetic energy retained.

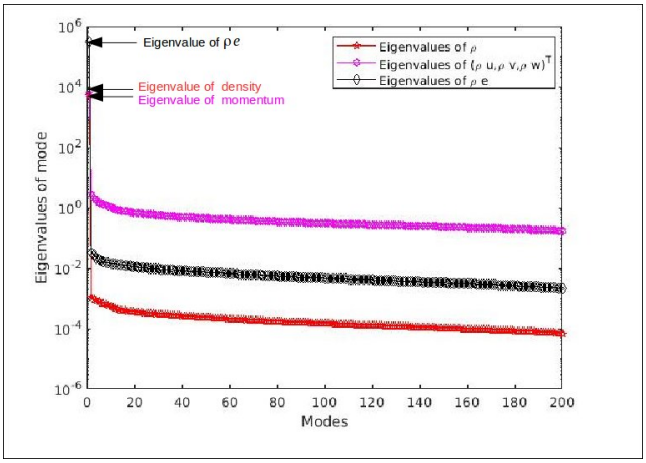

FIGURE 3 – Eigenvalues of (ρ) $(\rho u, \rho v, \rho w)^T$ and (ρe)

4.Results and analysis

The channel flow simulation was carried out in the reduced domain using the synthetic boundary condition described in the previous section. We first consider a boundary plane at an altitude of $z_0/H = 0.1$

above the solid wall (let say $2 - z_0/H = 0.1$, above the upper wall), corresponding to $z_{0+} = 18$. Simulations were run over a integration time corresponding to 72 time scales (H/U_0, where U_0 is the velocity at the middle of the channel. For this time interval, statistical quantities were computed and compared to those obtained in the reference (full) numerical domain. Averages were taken in time and in the homogeneous directions, *i.e.* in the x and y directions :

$$< q > (z) = \frac{1}{N_t \times L_x \times L_y} \sum_t \int_{x,y} q(x, y, z, t) dx dy.$$

4.1 Turbulent Statistics

The computing time for 72 nondimensional time units was 40 hours in reduced channel ($z_+ = 18$), however it would use 96 hours for the same duration of simulation in DNS. The mesh in reduced channel is $Nx \times Ny \times Nz = 97 \times 97 \times 85$, which is less than the mesh in DNS($Nx \times Ny \times Nz = 97 \times 97 \times 129$).

The mean streamwise velocity profile ($< u >$) is very well reproduced, especially in the inertial region where the log-law is clearly recovered (Fig. 4) in both parts of the channel, with a slight overprediction of 1.9 % throughout the channel.

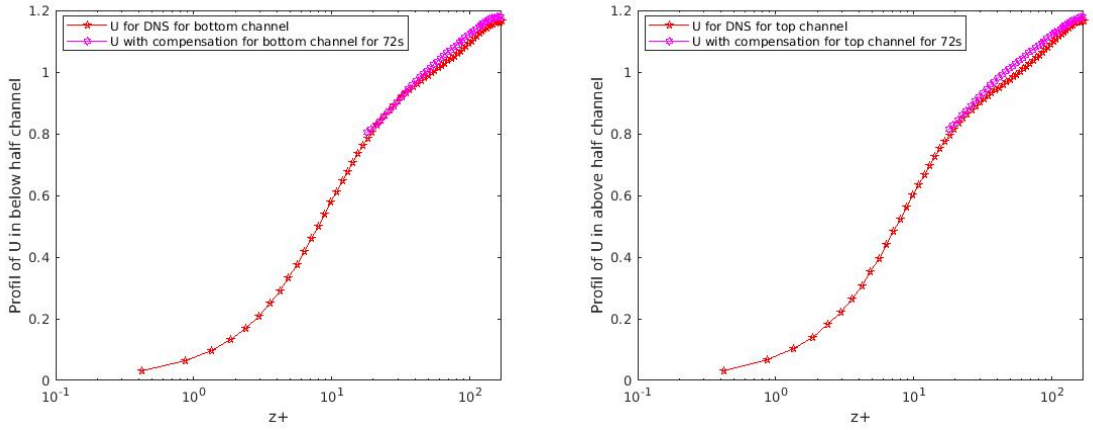

FIGURE 4 – Reduced channel flow with synthetic boundary conditions at $z = 0.1$ and $z = 1.9$. Profile of the mean streamwise velocity $< u >$ versus the normal to the wall direction (z) : the lower part of the channel in the left, and the upper part in the right. DNS values with red stars, reduced channel using the synthetic boundary conditions with magenta diamond.

With a slight overprediction of 0.1 % throughout the channel, the density profile also matches very well the DNS results (Fig. 5). These results demonstrate that the mean field is well predicted overall.

The shear stress (Fig. 5) is also correctly predicted, except for a region close to the boundary plane. The underprediction of the stress there corresponds to a local lack of correlation between the streamwise and the wall-normal coomponents, which could be linked to a lack of representativity of the POD basis used to represent the flow. The fact that the shear stress recovers the DNS profile in the center of the domain is consistent with the good prediction of the log-law distribution in the mean streamwise velocity profile (Fig. 4).

However other second-order statistics such as the turbulent intensities are over-predicted and steadily increase with the integration time. After 72 time units, the streamwise turbulent intensity ($< u'^2 >$)

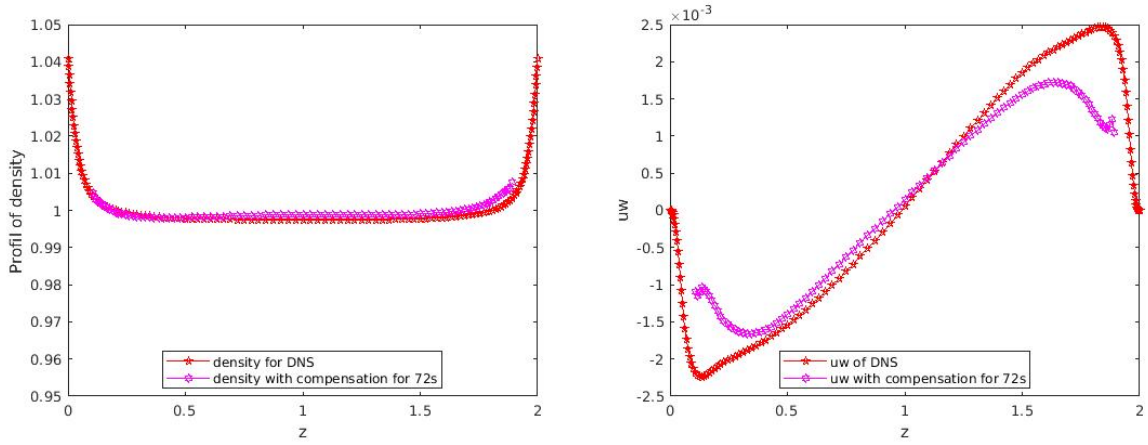

FIGURE 5 – Reduced channel flow with synthetic boundary conditions at $z = 0.1$ and $z = 1.9$. Profile of the mean density $< \rho >$ across the channel (versus z) in the left ; Profile of the shear stress $u'w'$ in the right . DNS values with red stars, reduced channel using the synthetic boundary conditions with magenta diamond.

is overpredicted by 26.75 %, the spanwise turbulent intensity ($< v'^2 >$) is overpredicted by 31.52 %, and the wall normal turbulent intensity ($< w'^2 >$) is largely overpredicted by 70 %. Consequently, the correlation between the longitudinal and the wall-normal fluctuations is correctly recovered, despite an excess of energy in the fluctuations.

4.2 Spectral analysis

To better understand and characterize the discrepancy between the reference and the reduced channel, spatial spectra have been computed at different heights.

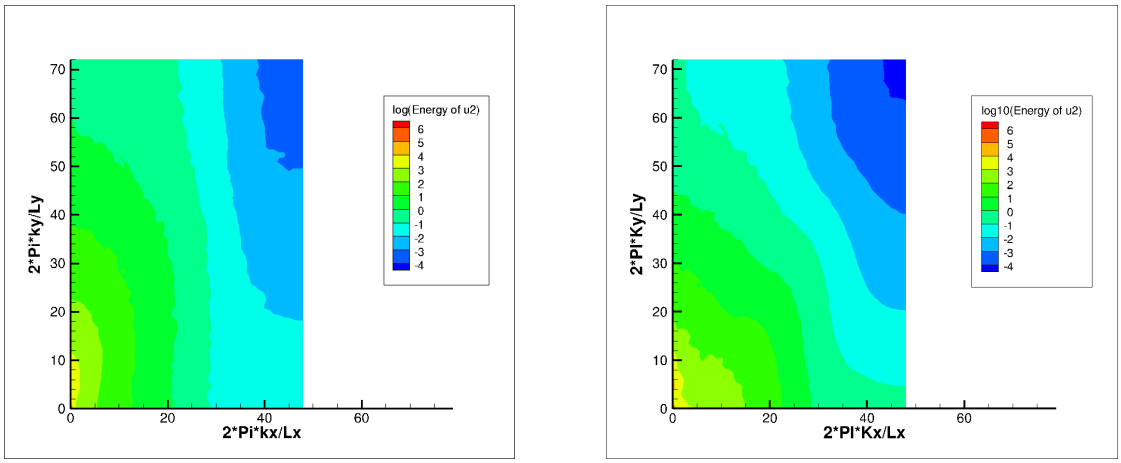

FIGURE 6 – Power density spectra of the streamwise velocity u on a plane at an altitude $z = 0.2$ versus the wave numbers in x and y directions : left in full channel and right in the reduced channel.

Power density spectra of the velocity components at an altitude $z = 0.2$ ($z^+ = 36^+$) are presented as a function of the streamwise and spanwise wavenumber in figure 6, 7, and 8 for both the DNS channel flow and the reduced channel. The integration time was 72 time scales. The general distribution of the kinetic energy in the DNS spectra is rather well recovered in the reduced channel simulation. We can however notice a shift of the kinetic energy towards greater wave numbers in the reduced channel, mainly in the longitudinal direction. This means that POD reconstructed synthetic boundary conditions seem to inject

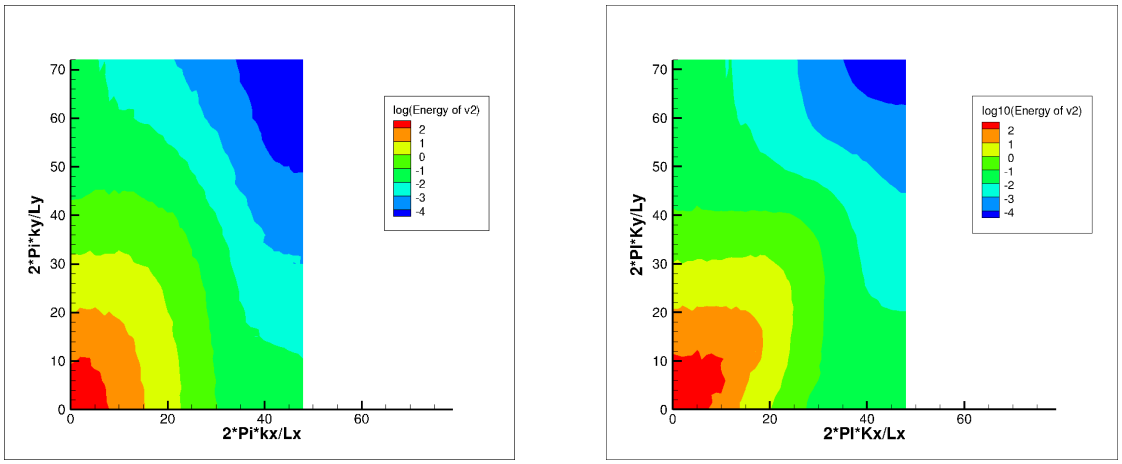

FIGURE 7 – Power density spectra of the spanwise velocity v on a plane at an altitude $z = 0.2$ versus the wave numbers in x and y directions : left in full channel and right in the reduced channel.

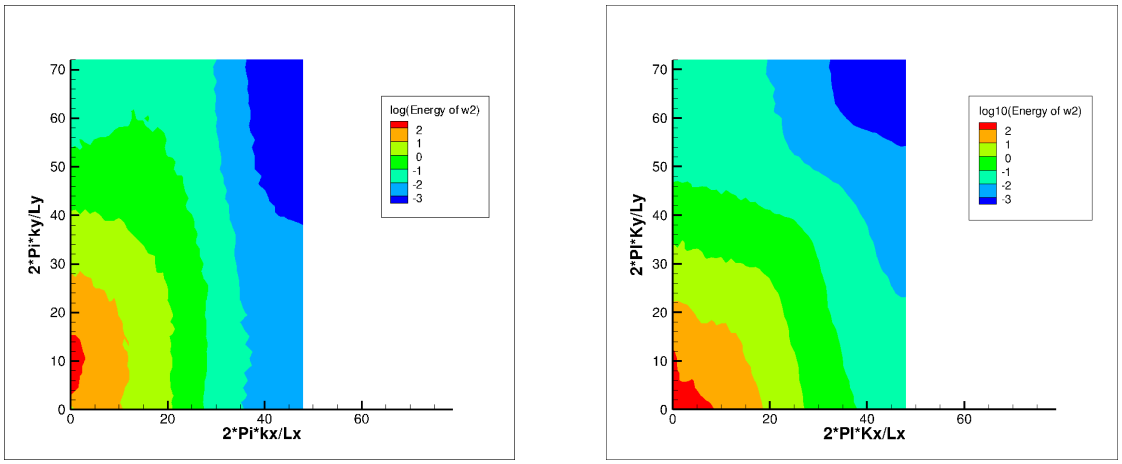

FIGURE 8 – Power density spectra of the normal to the wall velocity w on a plane at an altitude $z = 0.2$ versus the wave numbers in x and y directions : left in full channel and right in the reduced channel.

additional kinetic energy into smaller streamwise length scales. The shift is clearly noticeable in spectra of the longitudinal (Fig. 6) and normal to the wall components (Fig. 8) of the velocity and explains the over-prediction of the rms values of the velocity.

4.3 Results at a height of $z_+ \sim 50$

To study the robustness of the procedure, we also applied the POD synthetic boundary conditions on boundary planes at a higher altitude $z/H = 0.3$ and $2 - z/H = 0.3$, corresponding to $z^+ = 54^+$. The simulation was integrated over 36 time scales from an initial condition corresponding to fully developed turbulence. The computational time for 36 nondimensional time units was around 14 hours in the reduced channel($z_+ = 54$), versus 48 hours for the same duration of simulation in DNS. The mesh in reduced channel is $Nx \times Ny \times Nz = 97 \times 97 \times 53$, which is much less than the mesh in DNS($Nx \times Ny \times Nz = 97 \times 97 \times 129$).

The DNS mean streamwise velocity profile is recovered in the reduced channel even if the boundary plane lies well within the buffer region (Fig. 9). The log-law is very well recovered and the mean velocity is recovered in the reduced channel with an error throughout the channel less than 1 %. The density profile obtained in the reduced channel also matches very well the DNS results with less than 0.12 %

error throughout the channel (Fig. 10).

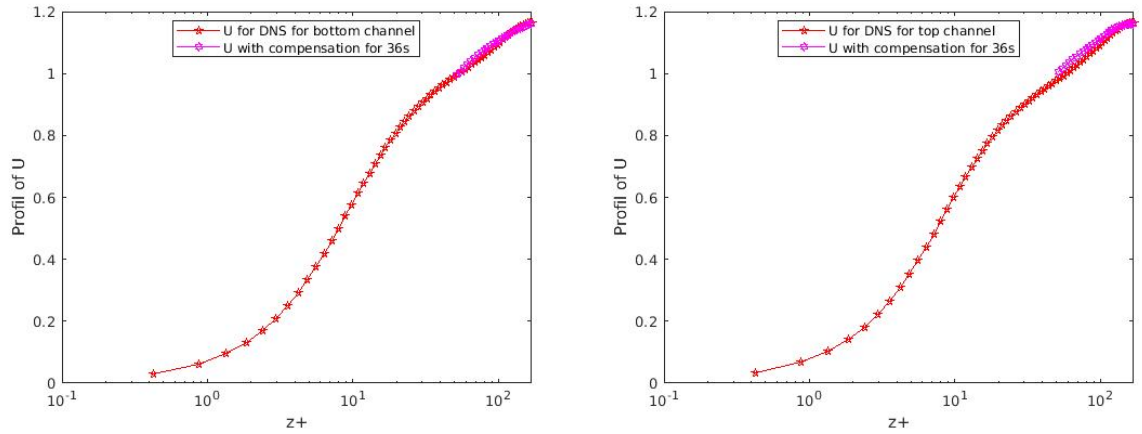

FIGURE 9 – Reduced channel flow with synthetic boundary conditions at $z = 0.3$ and $z = 1.7$. Profile of the mean streamwise velocity $< u >$ versus the normal to the wall direction (z) : the lower part of the channel in the left, and the upper part in the right. DNS values with red stars, reduced channel using the synthetic boundary conditions with magenta diamond.

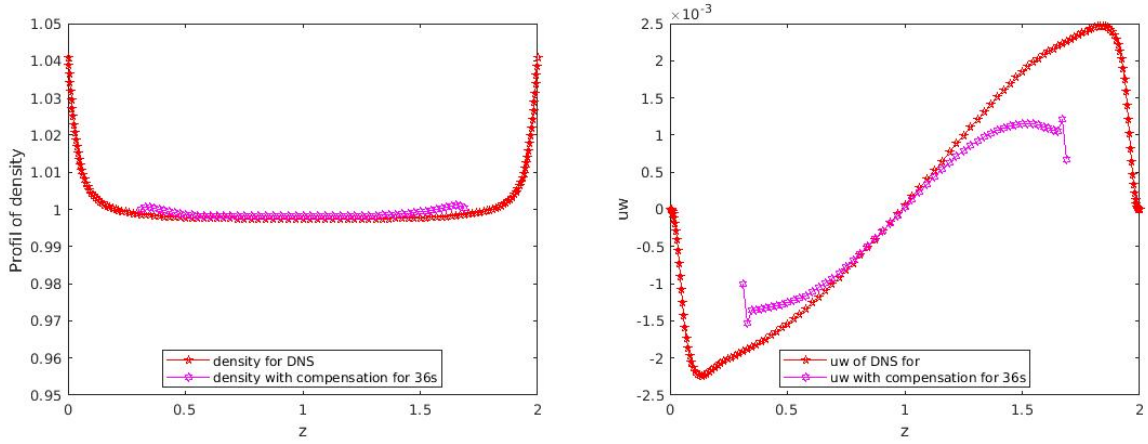

FIGURE 10 – Reduced channel flow with synthetic boundary conditions at $z = 0.3$ and $z = 1.7$. Profile of the mean density $< \rho >$ across the channel (versus z) in the left ; Profile of the shear stress $u'w'$ in the right. DNS values with red stars, reduced channel using the synthetic boundary conditions with magenta diamond.

As observed above, the shear stress (see Fig. 10) is also well predicted. Similarly as the first case, the shear stress profile exhibits a lack of correlation close to the boundary planes while the DNS results are recovered in the center of the channel. Large discrepancies on the turbulent intensities are recorded in the center of the channel : $rms(u)$ is overpredicted by 27.4 %, $rms(v)$ by 26 %, and $rms(w)$ is overpredicted by 66.2 % throughout the channel, which is quite similar to the previous results for however a smaller time integration. The procedure is therefore robust with respect to the boundary height.

5. Conclusion

We have investigated a procedure for the generation of synthetic wall boundary conditions for compressible flows. The reconstruction procedure is based on Proper Orthogonal Decomposition. A key element

is the estimation of POD amplitudes at each time step for *a priori* determined spatial POD modes. The procedure was tested for turbulent channel flow at $R_\tau = 180$. The full domain is replaced by a reduced domain in which the influence of the wall layer is felt through a virtual boundary plane where synthetic boundary conditions are imposed. Two boundary planes $y_+ \sim 20$ and $y_+ \sim 50$ were tested. Statistics and spatial spectra of the flow were computed in the reduced channel and compared with reference results in the full channel.

Results were found to be largely insensitive to the height of the boundary plane. However we found that the procedure was sensitive to the choice of the variables for the decomposition. The reason for this is not entirely clear and will require further investigation. By selecting the variables in an appropriate manner, we were able to recover the mean velocity profile within 2%. The Reynolds shear stress was also correctly predicted. However, the turbulent intensities tended to be overpredicted. Spectral analysis showed that this overprediction was due to excess energy at high streamwise wavenumbers. This issue could be addressed by filtering out the small scales over the full channel at regular intervals. We plan to examine such improvement strategies in future studies.

Références

[1] H. Choi and P. Moin. *Grid-point requirements for large eddy simulation : Chapmans estimates revisited*. Physics of Fluids **24** : 011702, 2012.

[2] G. I. Park and P. Moin. *An improved dynamic non-equilibrium wall-model for large eddy simulation*. Physics of Fluids **26** : 015108, 2014

[3] U. Piomelli and E. Balaras. *Wall-layer models for large-eddy simulations*. Annual Review of Fluid Mechanics **34** : 349–374, 2002 .

[4] G. N. Coleman, J. Kim and P. R. Spalart. *Direct numerical simulation of a decelerated wall-bounded turbulent shear flow*. J. Fluid Mech **495** : 1–18, 2003.

[5] C. P. Yorke and G. N. Coleman. *Assessment of common turbulence models for an idealized adverse pressure gradient flow*. European J. Mech. B Fluids **23** : 319–337, 2004.

[6] B. Podvin and Y. Fraigneau. *POD-based wall boundary conditions for the numerical simulation of turbulent channel flows*. Journal of Turbulence **15**, Issue 3, 2014.

[7] V. Daru and C. Tenaud. *High order one-step monotonicity-preserving schemes for unsteady compressible flow calculations*. Journal of Computational Physics, **193** : 563–594, 2004.

[8] C. Tenaud, B. Podvin, Y. Fraigneau and V. Daru, *On wall pressure fluctuations and their coupling with vortex dynamics in a separated–reattached turbulent flow over a blunt flat plate*. International Journal of Heat and Fluid Flow, **61**, Part B, 730–748, 2016.

[9] J. Kim, P. Moin and R. Moser. *Turbulence statistics in fully developed channel flow at low Reynolds number*. J. Fluid Mech, **177** : 133–166, 1987.

[10] Y. Mizuno and J. Jiménez *Wall turbulence without walls*. J.Fluid.Mech, **723** : 429–455, 2013

[11] Sirovich, L. *Turbulence and the Dynamics of Coherent Structures. Part 1 : Coherent Structures* Quarterly of Applied Mathematics, **45** 561–571, 1987